Exotic spin phases in two-dimensional spin-orbit coupled models: Importance of quantum effects

Chao Wang, Ming Gong,* Yongjian Han, Guangcan Guo, and Lixin He†
CAS Key Laboratory of Quantum Information, Chinese Academy of Sciences, University of Science and Technology of China, Hefei 230026, China
and Synergetic Innovation Center of Quantum Information and Quantum Physics, University of Science and Technology of China, Hefei 230026, China

(Received 24 January 2017; revised manuscript received 29 August 2017; published 12 September 2017)

We investigate the phase diagrams of the effective spin models derived from Fermi-Hubbard and Bose-Hubbard models with Rashba spin-orbit coupling, using string bond states, one of the quantum tensor network states methods. We focus on the role of quantum fluctuation effect in stabilizing the exotic spin phases in these models. For boson systems, and when the ratio between interparticle and intraparticle interaction $\lambda > 1$, the out-of-plane ferromagnetic (FM) and antiferromagnetic (AFM) phases obtained from quantum simulations are the same as those obtained from the classic model. However, the quantum order-by-disorder effect reduces the classical in-plane XY-FM and XY-vortex phases to the quantum X/Y-FM and X/Y-stripe phase when $\lambda < 1$. The spiral phase and skyrmion phase can be realized in the presence of quantum fluctuation. For the Fermi-Hubbard model, the quantum fluctuation energies are always important in the whole parameter regime. A general picture to understand the phase diagrams from a symmetry point of view is also presented.

DOI: 10.1103/PhysRevB.96.115119

I. INTRODUCTION

The ultracold atoms in an optical lattice [1–4] provide an excellent toolbox for simulating various spin models, such as Heisenberg [5] model, Kitaev model [6], etc., and has been one of the central concepts in quantum simulations. Along this line some primary results have been obtained [7–9]. The simplest ferromagnetic (FM) or antiferromatic (AFM) Heisenberg spin models can be obtained in the deep Mott phase regime [3] when the Hubbard model possesses rotational symmetry. The recent interest in the searching of exotic spin structures in optical lattice is stimulated by the experimental realization of spin-orbit coupling (SOC), which can be regarded as the simplest non-Abelian gauge potential in nature [10–27]. In these cases, the effective spin models may become more complicated due to the appearance of some exotic terms, e.g., the Dzyaloshinskii-Moriya (DM) [28,29] interactions and their deformations.

The DM interaction has already been widely investigated in solid materials [30–39] and now it is resurfaced in ultracold atoms due to its flexibility in experiments, e.g., the SOC interactions can be made much stronger than their counterpart in real materials. Results based on classical simulations [40–42], Ginzburg-Landau theory [43,44], dynamical mean-field theory [45], and spin wave expansion [46,47] have unveiled rich phase structures including spin spirals, skyrmions in the presence of the frustrated interactions caused by the SOC: there is strong competition between spin-independent tunneling and the SOC induced spin-flipping tunneling. It is well known that quantum fluctuations are greatly enhanced in low-dimensional systems, and therefore the ground state may differ significantly from the semiclassical orderings as in higher dimensions. Given the role of quantum fluctuation effects in the above two-dimensional models have not been thoroughly investigated, it is of great interest to see whether the phases predicted by the semiclassical theories can survive or new phases may emerge because of quantum fluctuation.

In this work we investigate the quantum phase diagrams of the effective spin models with Rashba SOC, derived from Bose-Hubbard (BH) model and Fermi-Hubbard (FH) model on a square lattice, using recently developed string bond states (SBS) [48], which is one of the tensor network states (TNS) methods [49–52]. The SBS used in this work satisfies area law [48,53], and thus can express the ground state of many interesting quantum systems effectively. We find, whereas in some parameters regions the classic spin model can give qualitatively correct ground states, in some regions, the quantum effects are crucial to get correct ground states. In particular, for the fermion systems, the quantum effects are always important.

II. EFFECTIVE SPIN MODELS

For a BH model with Rashba SOC, the Hamiltonian can be written as $H_{\mathrm{BH}} = \mathcal{H}_0 + \frac{U}{2}\sum_{i,\sigma} n_{i\sigma}(n_{i\sigma}-1) + \lambda U \sum_i n_{i\uparrow}n_{i\downarrow}$, where U and λU are on-site intraparticle and interparticle interactions and $\mathcal{H}_0 = -t\sum_{\langle i,j\rangle} \Psi_i^\dagger \exp[-i\alpha \mathbf{e}_z \cdot (\vec{\sigma}\times \mathbf{e}_{ij})]\Psi_j$. Here $\Psi^\dagger = (b_{i\uparrow}^\dagger, b_{i\downarrow}^\dagger)$, with $b_{i\sigma}^\dagger$ being the creation operator with site i and spin $\sigma = \uparrow,\downarrow$ and $\mathbf{e}_{ij}$ being the unit vector from site i to j. In the first Mott lobe ($U \gg t$), each site contains only one particle, the effective spin model can be written as

$$
\begin{aligned}
H = J\sum_{\langle i,j\rangle_x}\Bigg[&\frac{\cos(2\alpha)}{\lambda}S_i^xS_j^x + \frac{1}{\lambda}S_i^yS_j^y + \frac{\cos(2\alpha)}{\lambda}(2\lambda-1)S_i^zS_j^z \\
&- \sin(2\alpha)\left(S_i^xS_j^z - S_i^zS_j^x\right)\Bigg] + J\sum_{\langle i,j\rangle_y}\Bigg[\frac{1}{\lambda}S_i^xS_j^x \\
&+ \frac{\cos(2\alpha)}{\lambda}S_i^yS_j^y + \frac{\cos(2\alpha)}{\lambda}(2\lambda-1)S_i^zS_j^z \\
&- \sin(2\alpha)\left(S_i^yS_j^z - S_i^zS_j^y\right)\Bigg], \qquad (1)
\end{aligned}
$$

*gongm@ustc.edu.cn
†helx@ustc.edu.cn

where $J = -4t^2/U < 0$, and $\langle i,j\rangle_\mu$ means the nearest neighbors in the $\mu = x,y$ directions. In this model, α determines the strength of SOC, and λ represents the anisotropy of the exchange interactions. Similarly in the FH model, the Hamiltonian reads as $H_{\rm FH} = \mathcal{H}_0 + \sum_i U n_{i\uparrow} n_{i\downarrow}$, where $\mathcal{H}_0$ has the same form as the boson model with $\Psi^\dagger$ replaced by $(f^\dagger_{i\uparrow}, f^\dagger_{i\downarrow})$, where $f^\dagger_{i\sigma}$ is the fermion creation operator at site i and spin $\sigma = \uparrow,\downarrow$. The corresponding effective spin model is equal to that in Eq. (1) at $\lambda = 1$ except that now $J = 4t^2/U > 0$ due to Pauli exclusion principle. Hereafter we let $4t^2/U = 1$ for convenience.

The following order parameters are used to distinguish different phases. First, the static magnetic structure factor is defined as $[\mu = x,y,z, i = (i_x,i_y)]$

$$S^\mu(\mathbf{k}) = \frac{4}{L^2}\sum_{i,j}\left\langle S^\mu_i \cdot S^\mu_j\right\rangle e^{i[(i_x-j_x)k_x+(i_y-j_y)k_y]/L} \tag{2}$$

on a $L \times L$ square lattice. For the FM and AFM phases along μ direction, $S^\mu(\mathbf{k})$ has peaks at $\mathbf{k} = (0,0)$ and (π,π), respectively; and in the strip phase the strongest peaks happen at $\mathbf{k} = (0,\pi)$ or $(\pi,0)$. We also define the spiral and skyrmion order parameters in real space as [54]

$$\mathrm{Sp}_\mu(i,j) = 16\left\langle\theta^i_\mu\theta^j_\mu\right\rangle, \quad \mathrm{Sk}(i,j) = 64\left\langle v^i_s v^j_s\right\rangle, \tag{3}$$

where $\theta^i_x = (\mathbf{S}_i \times \mathbf{S}_{i+\mathbf{e}_x})_y$ and $\theta^i_y = (\mathbf{S}_i \times \mathbf{S}_{i+\mathbf{e}_y})_x$ are related to the relative planer spin angles for spins at site i and $i + \mathbf{e}_\mu$. To account for the three-dimensional spin alignment effect, we define the spin volume constructed by the spins at the three neighboring sites as $v^i_s = \mathbf{S}_i \cdot (\mathbf{S}_{i+\mathbf{e}_x} \times \mathbf{S}_{i+\mathbf{e}_y})$. In the coplanar spiral phase, $v^i_s = 0$ exactly, but it is nonzero in the skyrmion phases. To determine the long-range order of the system, we calculate the order parameters as

$$\mathrm{Sp}_\mu = \sum_i \frac{1}{L^2}|\mathrm{Sp}_\mu(i,i+l)|, \quad \mathrm{Sk} = \sum_i \frac{1}{L^2}|\mathrm{Sk}(i,i+l)|, \tag{4}$$

where $l = (L/2,L/2)$ to make $|i-j|$ as large as possible and i is averaged over the whole lattice for better numerical accuracy.

III. NUMERICAL METHOD

We explore the quantum spin models on a 12×12 lattice with periodic boundary condition, using the SBS method, which is a specific type of tensor network state (TNS) methods developed by Schuch *et al.* [48]. In this method, the SBS forms a systematically improvable variational space, controlled by the virtual bond dimensions. Once we have the SBS representation of the many-particle wave functions, the ground state energies as well as corresponding wave functions can be obtained variationally. We recently predict a peculiar supersolid phases induced by frustrated tunneling in the extended Bose-Hubbard model using this method [55].

The many-particle wave functions represented in SBS can be written as

$$|\Psi\rangle = \sum_{s_1\cdots s_N}\prod_{p\in\mathcal{P}}\mathrm{Tr}\left[\prod_{k\in p}A^{s_{n(k)}}_{p,k}\right]|s_1\cdots s_N\rangle, \tag{5}$$

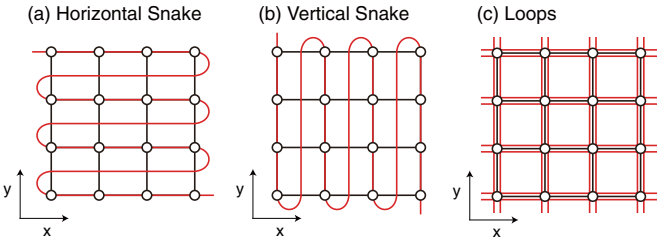

FIG. 1. Three types of strings included in the simulation: (a) a horizontal snake string, (b) a vertical snake string, and (c) the loops. The white circles stand for tensors locates on the 2D square lattice, whereas the red lines stand for the tensor virtual bonds that form strings.

where $\mathcal{P}$ is a certain string pattern which contains a set of strings p. In each string p, as illustrated in Fig. 1, we have an ordered list of tensors $A^s_{p,k}$, locate on the kth site of the string, which is the $n(k)$th site of the lattice. The tensor has a physical index s. The two nearby tensors are connected via the the virtual bonds, with bond dimension D. Therefore, each $A^s_{p,k}$ is a $d \times D \times D$ tensor, where $d = 2$ is the physical dimension (for spin), and the bond dimension D encodes the entanglement between the site and its environment. With increasing the bond dimension D, the SBS can systematically converge to the ground state.

We use the products of three types of string tensors: the horizontal snake string [Fig. 1(a)], the vertical snake string [Fig. 1(b)], and the loops [Fig. 1(c)]. Note that if we use only the horizontal snake string or the vertical snake string, the SBS reduces to the conventional matrix product state (MPS), which is equivalent to the widely used density matrix renormalization group (DMRG) method. However, since MPS does not satisfy the area law [48,53] in two dimensions, it is inefficient to simulate the two-dimensional problems.

For a given a Hamiltonian H, the total energy of the system is a function of the SBS tensors at each lattice site $A^s_{p,k}$, i.e., $E = E(\{A^s_{p,k}\})$. We recently developed an efficient algorithm to obtain the ground state wave function and corresponding energy by mapping the problem to optimizing the total energy of a classical mechanical system, in which the elements $a^s_{ij}(p,k)$ of the tensor $A^s_{p,k}$ are treated as the generalized coordinates of the system. We calculate the total energy and the energy gradients for a given SBS via Monte Carlo sampling [48,56] method. The ground state wave function and total energy are then obtained via a replica-exchange (also known as parallel tempering) [57,58] molecular dynamic simulation. The replica-exchange MD method can effectively avoid the system being trapped in local minima. In our simulations, we use $M = 42$ temperatures. Initially, the temperatures distribute exponentially between the highest $(1/\beta_0 = 10^{-4})$ and lowest $(1/\beta_{M-1} = 10^{-6})$ temperatures. For each temperature, we start from random tensors. During the simulations, we adjust the temperatures after configuration exchange ten times, whereas there are 200 MD steps between the two configuration exchanges, with a step length $\Delta t = 0.05$. For each MD step, we sample about 20 000 spin configurations. The energies used for temperature exchange are averaged over 200 MD steps. After we finish the replica-exchange MD optimization, we further decrease the temperature to 10^{-8} to obtain more

accurate results. Full details of the method are presented in our previous publication [56]. For the spin models, we use bond dimension $D = 8$ which converges the total energies with errors less than 10^{-4} per site.

IV. PHASE DIAGRAM FOR BOSON

The phase diagram is presented in Fig. 2 and corresponding order parameters are given in Fig. 3 at $\lambda = 1.5$ and $\lambda = 0.8$ and $\alpha \in [0,\pi/2]$. The spin model in Eq. (1) possesses some unique symmetries, which is crucial to understand this phase diagram. First, the Hamiltonian in Eq. (1) is invariant upon operation $\alpha \to \pi - \alpha$ and $S_i^{x,y} \to -S_i^{x,y}$, which is equivalent to the transformation $U_\uparrow^\dagger b_{i\uparrow} U_\uparrow = -b_{i\uparrow}$, where $U_\uparrow = \exp(i\pi \sum_i n_{i\uparrow})$ in the original BH model. This symmetry directly leads to $U_\uparrow^\dagger H(\alpha,\lambda)U_\uparrow = H(\pi-\alpha,\lambda)$, i.e., the phase

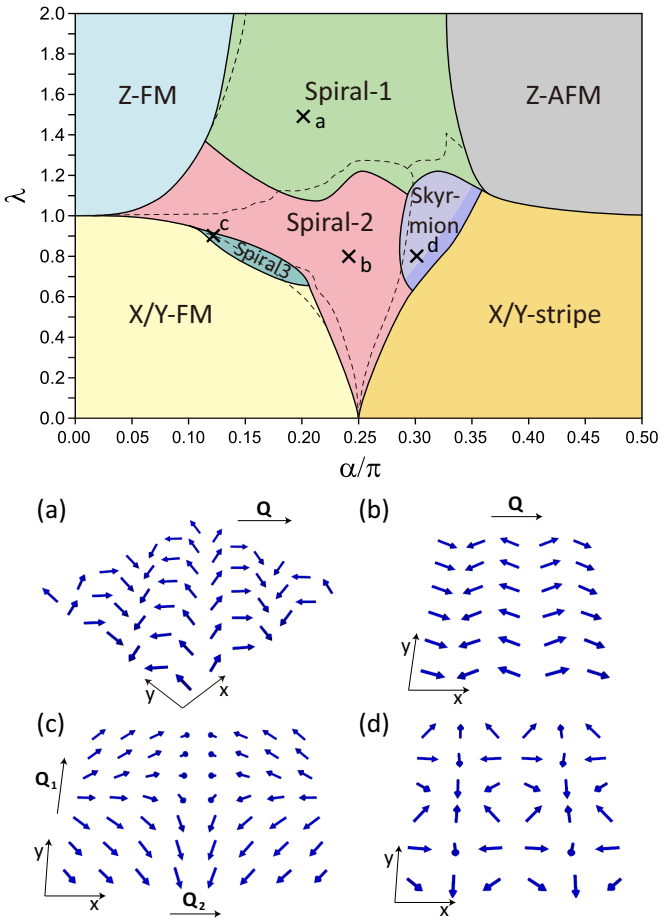

FIG. 2. Upper panel: Phase diagram for Eq. (1), calculated from TNS method. Z-FM (Z-AFM) denote the ferromagnetic (antiferromagnetic) phase with spin polarized along the z direction, and X/Y means that the spins are polarized along either x or y direction. For a comparison the phase boundaries determined by classical simulations are shown as dashed lines. Lower panel: Spin textures of (a) spiral-1 phase with spins spiral along $\mathbf{Q} = \mathbf{e}_x - \mathbf{e}_y$ direction, (b) spiral-2 phase with spins spiral along $\mathbf{Q} = \mathbf{e}_x$ direction, (c) spiral-3 phase spins spiral along both $\mathbf{Q}_1 = \mathbf{e}_y$ and $\mathbf{Q}_2 = \mathbf{e}_x$ directions, and (d) 3×3 skyrmion phase.

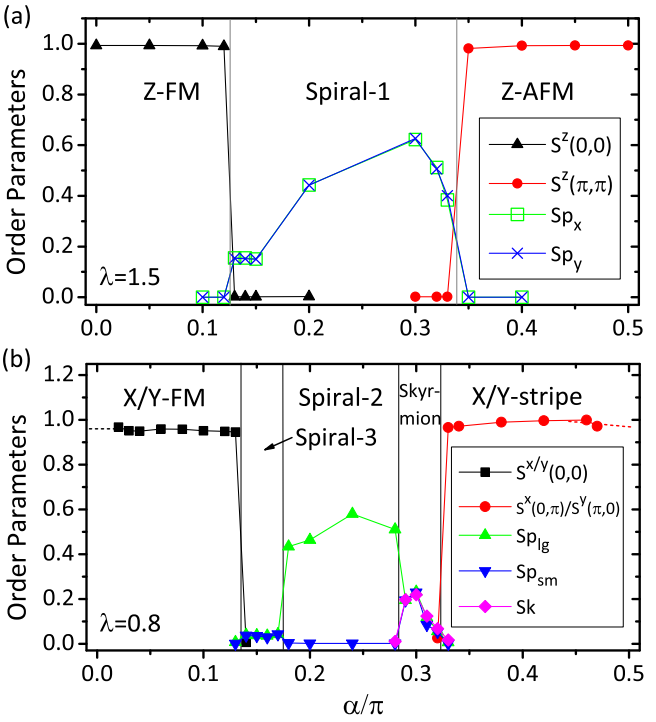

FIG. 3. Order parameters for the effective spin model derived from Bose-Hubbard model at (a) $\lambda = 1.5$ and (b) $\lambda = 0.8$, where Sp_{lg} [Sp_{sm}] is the larger (smaller) one of Sp_x and Sp_y (see text for details).

diagram should be symmetric about $\alpha = \frac{\pi}{2}$. Therefore, we only show the result for $\alpha \in [0,\pi/2]$.

We first discuss the phase diagram at four corners, where $\alpha \sim 0$ or $\pi/2$ and $\lambda \ll 1$ or $\lambda \gg 1$. When $\alpha = 0$, i.e., in the absence of SOC, the original spin model can be reduced to an effective XXZ spin model, with $J_x = J_y = -1/\lambda$, and $J_z = -(2\lambda - 1)/\lambda$. When $\lambda > 1$, $|J_z| > |J_x|$, the ground state is a Z-FM state, i.e., all spins are ferromagneticlly aligned along the z direction. Our TNS calculations show that for small $\alpha \lesssim 0.15$, the ground state is still Z-FM, as determined by the order parameters shown in Fig. 3(a). In this region, the quantum simulations yield the same ground state as the classic one, suggesting the minor role of quantum fluctuation effect.

Interestingly, at $\alpha = \frac{\pi}{2}$, the model can be mapped to the $\alpha = 0$ case via a symmetry transformation $\mathcal{U} = \prod_i e^{-i\frac{\pi}{2} i_x \sigma_x} e^{-i\frac{\pi}{2} i_y \sigma_y}$, i.e., $\mathcal{U}^\dagger H_{\frac{\pi}{2}} \mathcal{U} = H_0$. Use this transformation, we immediately see that the ground state near $\alpha = \frac{\pi}{2}$ is a Z-AFM. We therefore see that these two limits ($\alpha = 0$ and $\alpha = \frac{\pi}{2}$) should have the exact same energies, and the quantum effects are small in both phases, which are confirmed by the numerical results.

However, there are dramatic differences in the case of $\lambda < 1$ where the in-plane exchange energy dominates. The order parameters calculated by TNS at $\lambda = 0.8$ are shown in Fig. 3. In the region of $0 < \alpha/\pi < 0.13$, the ground state is a FM phase, where all spins are polarized along either x or y direction, which we denote as X/Y-FM phase. Remarkably this phase is very different from what is obtained from the classical spin model, which gives a rotational invariant FM state [41] where all spins lay in the x-y plane (dubbed as XY-FM). To

understand this difference, we note that the in-plane rotational symmetry is not inherent of the original Hamiltonian, which possesses only C_4 symmetry. The rotational invariance of the ground state in the classic model is due to the accidental degeneracy because the ground state of the classic model happens to have $S_z = 0$. When quantum fluctuation is introduced, it breaks the accidental degeneracy and restores the C_4 symmetry of the original Hamiltonian, which therefore singles out a ground state with lower energy than the classical solution. This is the known as order-by-disorder mechanism [59,60]. Again, we can apply symmetry transformation $\mathcal{U} = \prod_i e^{-i\frac{\pi}{2}i_x\sigma_x} e^{-i\frac{\pi}{2}i_y\sigma_y}$ near $\alpha = \pi/2$, which yields a X/Y-stripe phase (as confirmed by numerical results) for a quantum spin model, in contrast to the 2×2 vortex state obtained from classical simulations.

The line $\lambda = 0$ in principle cannot he achieved due to the energy-costless double occupation. However, this limit can still be defined in the sense of $\lim_{\lambda\to 0} \lambda H_\lambda = -\sum_{\langle i,j\rangle_x} [\cos(2\alpha)(S_i^x S_j^x + S_i^z S_j^z) + S_i^y S_j^y] - \sum_{\langle i,j\rangle_y} [\cos(2\alpha)(S_i^y S_j^y + S_i^z S_j^z) + S_i^x S_j^x]$. Obviously when $\alpha = \frac{\pi}{4}$,

$$\lim_{\lambda\to 0} \lambda H_{\lambda,\alpha=\frac{\pi}{4}} = -\left(\sum_{\langle i,j\rangle_x} S_i^y S_j^y + \sum_{\langle i,j\rangle_y} S_i^x S_j^x\right), \qquad (6)$$

which gives a compass model due to the strong coupling between the spins and directions [61]. This model cannot be solved exactly; however, it can be shown exactly that the ground state is 2^{L+1}-fold degenerated for a $L \times L$ square lattice [62–64]. It therefore corresponds to a critical boundary between the X/Y-FM and X/Y stripe phases since any deviation from this critical point by varying the parameters (λ and α) can break the degeneracy and open an energy gap. The classical and quantum simulations yield the same critical point.

We next try to understand the spiral and skyrmion phases in the presence of strong DM interaction. The order parameters are shown in Eq. (4) (and the corresponding spin textures are shown in the lower panel of Fig. 2). The spiral-1 phase has two degenerate states spiral along either $\mathbf{e}_x + \mathbf{e}_y$ or $\mathbf{e}_x - \mathbf{e}_y$ direction. For these two cases the strongest peaks in the structure factor $S(\mathbf{k})$ appear at $\mathbf{k} = \pm(k_0, k_0)$ and $\mathbf{k} = \pm(k_0, -k_0)$, respectively, where k_0 can be smoothly tuned by α and λ. However, due to the finite size used in the simulation, only $k_0 = \frac{2\pi}{3}, \frac{\pi}{2}, \frac{\pi}{3}$, and $\frac{\pi}{6}$ are observed, which are commensurate with the system size. In this phase, the skyrmion order Sk ~ 0, whereas $\mathrm{Sp}_x = \mathrm{Sp}_y \neq 0$ are strongest among all the order parameters. The spiral-2 phase has two degenerate states, one is a spin spiral along x direction, and other one is along y direction. Therefore, only one of the order parameters, either Sp_x or Sp_y [see Fig. 3(b)], is nonzero. In contrast, in spiral-3 phase, $\mathrm{Sp}_x = \mathrm{Sp}_y$, both are nonzero. Spiral-3 phase is also observed in the classical model, and compared to the classical model, the spiral-3 phase region is greatly suppressed in the quantum model. It is worth noting that the spiral-3 phase was missing in Ref. [41]. One possible reason for the difference is that we use very high precision in the classical simulations in which the relative energy errors are about 10^{-5} compared to 10^{-2} in Ref. [41]. In the skyrmion phase, the structure factor exhibits strongest peaks at $\mathbf{k} = (\pm k_0, 0)$ and $(0, \pm k_0)$. Furthermore, the noncoplanar of spin alinement induces a

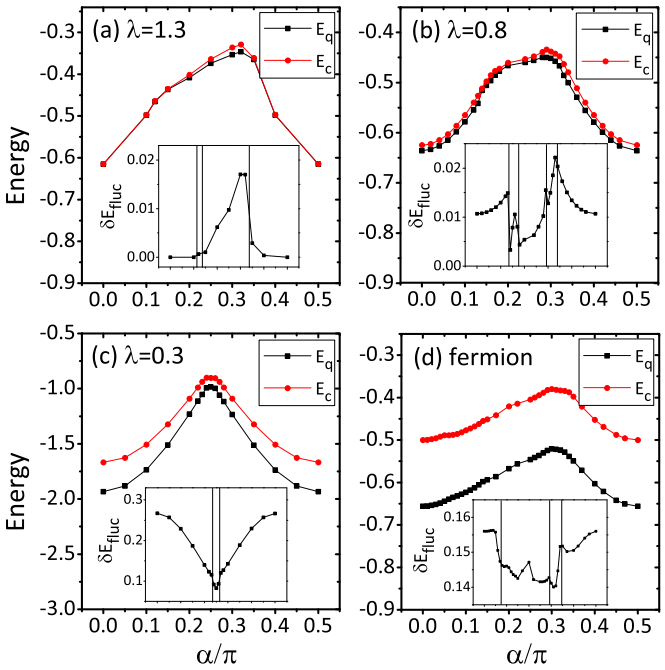

FIG. 4. Ground state energies from the classical (E_c) and quantum (E_q) simulations at (a) $\lambda = 1.3$, (b) $\lambda = 0.8$, and (c) $\lambda = 0.3$ for boson, and (d) for fermion models. Insets give the corresponding fluctuation energy δE_{fluc}. The vertical lines are the phase boundaries calculated by TNS.

finite skyrmion order Sk. The skyrmion phase is Néel type [65] and has a period 3×3 (light purple region in Fig. 2) or larger (dark purple region in Fig. 2), which is consistent with the numerical results for the classic spin model [41].

To understand the quantum effects in a more quantitative way, we plot the ground state energies per site for $\lambda = 1.3, 0.8, 0.3$ in Figs. 4(a)–4(c), respectively, obtained from classical simulations (E_c) and full quantum mechanical TNS simulations (E_q). In the inserts, we also show the energy differences

$$\delta E_{\mathrm{fluc}} = E_c - E_q\,. \qquad (7)$$

Obviously $E_c \geqslant E_q$, thus $\delta E_{\mathrm{fluc}} \geqslant 0$. From Fig. 4(a) we find that when $\alpha = 0$, and $\lambda = 1.3$, $E_c = -0.61537$, and $E_q = -0.61538$ in the 12×12 lattice, while the exact classical energy in a infinite size system is $E_c^\infty = \frac{2\lambda-1}{2\lambda} = -0.61538$. This agreement can be understood as follows: at $\alpha = 0$, the original model Eq. (1) reduces to a XXZ model (see the Appendix) with $J = -1$, and when $\lambda > 1$, the product state (Z-FM) is the exact ground state, and therefore $\delta E_{\mathrm{fluc}} = 0$ exactly. In fact the XXZ model can be used as a benchmark for the TNS method, which shows great accuracy in this problem. As shown in Fig. 4(a), $\delta E_{\mathrm{fluc}} \sim 0$ in the whole Z-FM and Z-AFM phase regimes, even when $\alpha \neq 0$. In the spiral phase, $\delta E_{\mathrm{fluc}} \sim 0.01$–$0.02$ is more significant.

The fluctuation energy increases with the decreasing of λ. At $\lambda = 0.8$, $\delta E_{\mathrm{fluc}} \sim 0.01$ in the X/Y-FM and X/Y strip phases, which is about 4% of the total energies. However, even though this energy difference seems not very large, the ground states predicted by classical model and quantum model are totally different. Full quantum treatments are therefore required to

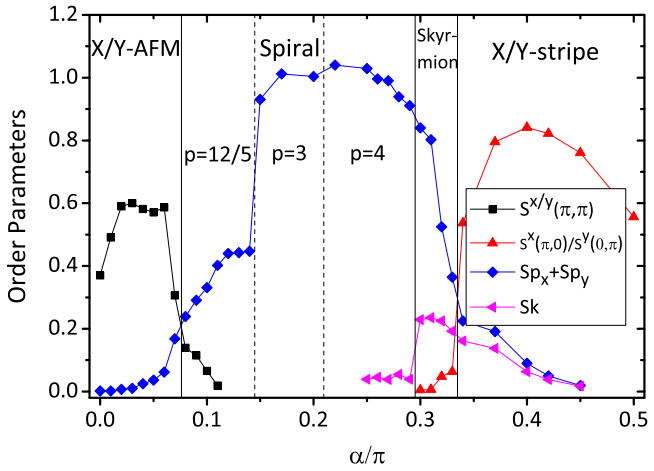

FIG. 5. Order parameters for the effective spin model derived from the Fermi-Hubbard model.

capture the correct physics in these phases. δE_{fluc} is also different for different phases, which is most significant in the skyrmion phase, where $\delta E_{\text{fluc}} \sim 0.02$. When λ further decrease to 0.3, δE_{fluc} increases dramatically. It is about 0.1–0.3 in the X/Y-FM and X/Y strip phases, which counts almost 10%–20% of the total energies. The strong quantum fluctuation at small λ suppresses the spiral-3 and skyrmion phases compared to the the classical phase diagram (see Fig. 2).

V. PHASE DIAGRAMS FOR FERMION

For the spin model from FH model, we have $J = 4t^2/U > 0$, and $\lambda = 1$. Therefore, α serves as the only adjustable parameter in this model. The calculated phase diagram and the order parameters from the TNS method are presented in Fig. 5. Similar to the phase diagrams in the bosonic system, we find X/Y-AFM phase when $\alpha/\pi < 0.08$ and X/Y-stripe phase when $\alpha/\pi \in [0.34,0.5]$ (the mirror symmetry about $\alpha = \frac{\pi}{2}$ is assumed). As before the classical model predicts a rotational invariant AFM and vortex phases in the x-y plane, which reduce to the X/Y-AFM and X/Y-stripe phase due to order-by-order effect. Between the AFM and stripe phases, there are spiral phases and one skyrmion phase. The spiral phase may also be distinguished by the period $p = \frac{12}{5}$, 3, 4 which can be accommodated by our simulation sizes. In these phases the skyrmion order almost equal to zero and the spiral order dominates. However, when $\alpha/\pi \in [0.29,0.34]$, the skyrmion order become important although the spiral order is still nonzero, similar to that in Fig. 3(b).

The quantum fluctuation energy is much more pronounced in the FH model than in the BH model for all phases, as depicted in Fig. 4(d). For $\alpha = 0$ we find $E_c = -0.5$, and $E_q = -0.6579$, thus $\delta E_{\text{fluc}} = 0.1579$. In the AFM and strip phases, δE_{fluc} is about 30% of the total energy. The large quantum fluctuation energy in the AFM state is due to that there are vast Hilbert spaces near the $S = 0$ that are energetically close to the ground state. The δE_{fluc} is slightly small in the spiral phase and skyrmion phase, but still significant.

It is very interesting to note that the Z-AFM state in BH model however has very small δE_{fluc}, in sharp contrast with the AFM state derived from the FH model. To understand this difference, we note that the Z-AFM state in BH model can be mapped to the Z-FM state via symmetry transformations, which has small quantum fluctuation energy. Therefore, even though the two AFM states appear very similar to each other at the *classical* level, their physics are entirely different. More fundamentally, this difference is rooted from the different statistic properties between bosons and fermions.

VI. CONCLUSION

We address the role of quantum fluctuation effect on the possibilities on observing the exotic spin structures in the spin-orbit coupled BH and FH models on a square lattice using TNS method. While for the out-of-plane FM and AFM phases the classical and quantum solution are the same, we find that the quantum order-by-disorder effect reduces the classical in-plane XY-FM and XY-vortex phases to the quantum X/Y-FM and X/Y-stripe phase. Moreover, the spiral phase and skyrmion phase can still be found even in the presence of quantum fluctuating effect. The structure of the phase diagrams are also understood from the symmetry point of view.

ACKNOWLEDGMENTS

This work was funded by the Chinese National Science Foundation Grants No. 11374275 and No. 11474267, and the National Key Research and Development Program of China Grant No. 2016YFB0201202. M.G. acknowledges the support by the National Youth Thousand Talents Program No. KJ2030000001, the USTC start-up Funding No. KY2030000053, and the CUHK RGC Grant No. 401113. The numerical calculations have been done on the USTC HPC facilities. M.G. thanks W. L. You for valuable discussions about the compass model.

APPENDIX: HOLSTEIN-PRIMARKOV TRANSFORMATION FOR THE XXZ MODEL

At $\alpha = 0$ the original model Eq. (1) in the main text reduces to a XXZ model,

$$\lambda H = -\sum_{\langle i,j\rangle} \left[S_i^x S_j^x + S_i^y S_j^y + (2\lambda - 1) S_i^z S_j^z\right]. \tag{A1}$$

We solve the effective XXZ model, using the Holstein-Primarkov (HP) method [66]. We consider first the case of $\lambda > 1$. When $\lambda > 1$, the spin is fully polarized along the z direction in the classical simulation, based on which we perform HP transformation,

$$S_i^z = S - n_i = \frac{1}{2} - n_i, \tag{A2}$$

$$S_i^x = \frac{1}{2}(\sqrt{2S - n_i}\, a_i + a_i^\dagger \sqrt{2S - n_i}) \approx \frac{1}{2}(a_i + a_i^\dagger), \tag{A3}$$

$$S_i^y = \frac{i}{2}(-\sqrt{2S - n_i}\, a_i + a_i^\dagger \sqrt{2S - n_i}) \approx \frac{i}{2}(-a_i + a_i^\dagger). \tag{A4}$$

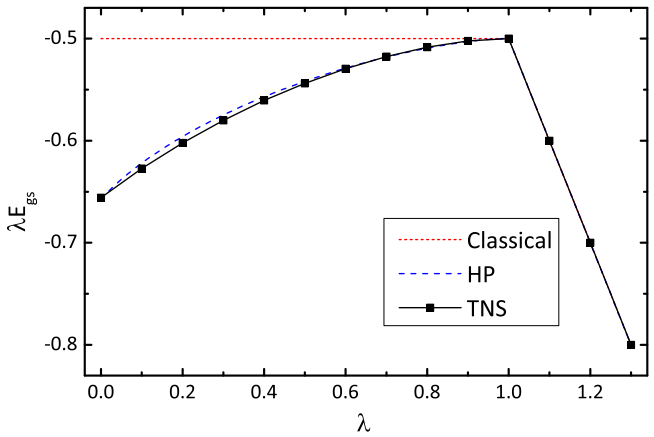

FIG. 6. Comparison between the ground state energies calculated by the classical model, HP method, and SBS method for the two-dimensional XXZ model.

By keeping the leading quadratic terms we find

$$\lambda H = -\frac{1}{2}\sum_{\langle i,j\rangle}[a_i^\dagger a_j + \text{H.c.}] - (2\lambda - 1)\sum_i \left[\frac{1}{2} - 2a_i^\dagger a_i\right]. \tag{A5}$$

After direct diagonalization of the above model we have the ground state energy (per site),

$$\lambda E_{\text{q}}^{\text{HP}} = \tfrac{1}{2} - \lambda, \tag{A6}$$

which is exactly the ground state energy for the classical model. It can be proved that the HP method gives the exact quantum energy when $\lambda > 1$. Therefore, when $\lambda > 1$, the quantum fluctuation energy $\delta E_{\text{fluc}} \sim 0$ in this model.

When $\lambda < 1$, the spins are polarized in the x-y plane, for instance, along x direction (the model has rotation symmetry in the x-y plane), we thus make a different HP transformation,

$$S_i^x = S - n_i = \frac{1}{2} - n_i, \tag{A7}$$

$$S_i^y = \frac{1}{2}(\sqrt{2S - n_i}a_i + a_i^\dagger\sqrt{2S - n_i}) \approx \tfrac{1}{2}(a_i + a_i^\dagger), \tag{A8}$$

$$S_i^z = \frac{i}{2}(-\sqrt{2S - n_i}a_i + a_i^\dagger\sqrt{2S - n_i}) \approx \frac{i}{2}(-a_i + a_i^\dagger). \tag{A9}$$

The Hamiltonian becomes

$$\lambda H = -\sum_i \left[\frac{3}{2} - (a_i a_i^\dagger + \text{H.c.})\right] - \sum_{\langle i,j\rangle}\left[\frac{\lambda}{2}(a_i^\dagger a_j + \text{H.c.}) + \frac{1-\lambda}{2}(a_i^\dagger a_j^\dagger + \text{H.c.})\right]. \tag{A10}$$

Different from Eq. (A5), in the above equation we now have pairing terms $a_i^\dagger a_j^\dagger$, which are beyond the classical models. Transferring the above equation to momentum space we have

$$\lambda H = -\frac{3}{2}N + \frac{1}{2}\sum_{\mathbf{k}}\{[2-\lambda(\cos k_x + \cos k_y)](a_{\mathbf{k}}^\dagger a_{\mathbf{k}} + a_{-\mathbf{k}}a_{-\mathbf{k}}^\dagger) + (\lambda - 1)(\cos k_x + \cos k_y)(a_{\mathbf{k}}^\dagger a_{-\mathbf{k}}^\dagger + \text{H.c.})\}. \tag{A11}$$

By performing Bogoliubov transformation,

$$\begin{pmatrix}\gamma_{\mathbf{k}}\\ \gamma_{-\mathbf{k}}\\ \gamma_{\mathbf{k}}^\dagger\\ \gamma_{-\mathbf{k}}^\dagger\end{pmatrix} = \begin{pmatrix}u & 0 & 0 & -v\\ 0 & u & -v & 0\\ 0 & -v & u & 0\\ -v & 0 & 0 & u\end{pmatrix}\begin{pmatrix}a_{\mathbf{k}}\\ a_{-\mathbf{k}}\\ a_{\mathbf{k}}^\dagger\\ a_{-\mathbf{k}}^\dagger\end{pmatrix}, \tag{A12}$$

where u and v satisfy

$$uv = \frac{(1-\lambda)(\cos k_x + \cos k_y)}{2\sqrt{[2-\lambda(\cos k_x + \cos k_y)]^2 - (1-\lambda)^2(\cos k_x + \cos k_y)^2}}, \tag{A13}$$

$$u^2 + v^2 = \frac{2 - \lambda(\cos k_x + \cos k_y)}{2\sqrt{[2-\lambda(\cos k_x + \cos k_y)]^2 - (1-\lambda)^2(\cos k_x + \cos k_y)^2}}, \tag{A14}$$

$a_{\mathbf{k}}$ and $a_{-\mathbf{k}}^\dagger$ are transformed into new bosonic operators $\gamma_{\mathbf{k}}$ and $\gamma_{-\mathbf{k}}^\dagger$,

$$\lambda H = -\frac{3}{2}N + \frac{1}{2}\sum_{\mathbf{k}}\sqrt{4 - 4\lambda(\cos k_x + \cos k_y) + (2\lambda - 1)(\cos k_x + \cos k_y)^2}\,(\gamma_{\mathbf{k}}\gamma_{\mathbf{k}}^\dagger + \gamma_{-\mathbf{k}}^\dagger\gamma_{-\mathbf{k}}). \tag{A15}$$

Therefore, the ground state energy calculated by HP method is

$$\lambda E_{\text{q}}^{\text{HP}} = -\frac{3}{2} + \frac{1}{8\pi^2}\int d\mathbf{k}\sqrt{4 - 4\lambda(\cos k_x + \cos k_y) + (2\lambda - 1)(\cos k_x + \cos k_y)^2}. \tag{A16}$$

The ground state energy of the classical model is calculated as

$$\lambda E_{\text{c}} = -\tfrac{1}{2}, \tag{A17}$$

which is a constant.

We compare the ground state energies λE_{gs} as functions of λ calculated by the classical model, the HP method, and the SBS method in Fig. 6. The results show that above $\lambda > 1$, the ground state energies obtained from the above three methods are almost identical, suggesting the quantum effects in this region are negligible. However, when $\lambda < 1$, the energy differences become obvious. The ground state energies calculated by the HP method and SBS method are much lower than those calculated by the classical model, revealing the importance of the quantum effects and with the decreasing of

λ the quantum effects become more pronounced. We note that the ground state energies calculated by SBS are even lower than those calculated by the HP method, which ignores the higher-order terms.

[1] D. C. McKay and B. DeMarco, Rep. Prog. Phys. **74**, 054401 (2011).
[2] I. Bloch, J. Dalibard, and W. Zwerger, Rev. Mod. Phys. **80**, 885 (2008).
[3] M. Greiner, O. Mandel, T. Esslinger, T. W. Hansch, and I. Bloch, Nature (London) **415**, 39 (2002).
[4] D. Jaksch, C. Bruder, J. I. Cirac, C. W. Gardiner, and P. Zoller, Phys. Rev. Lett. **81**, 3108 (1998).
[5] A. B. Kuklov and B. V. Svistunov, Phys. Rev. Lett. **90**, 100401 (2003).
[6] L.-M. Duan, E. Demler, and M. D. Lukin, Phys. Rev. Lett. **91**, 090402 (2003).
[7] D. Greif, T. Uehlinger, G. Jotzu, L. Tarruell, and T. Esslinger, Science **340**, 1307 (2013).
[8] K. Kim, M.-S. Chang, S. Korenblit, R. Islam, E. Edwards, J. Freericks, G.-D. Lin, L.-M. Duan, and C. Monroe, Nature (London) **465**, 590 (2010).
[9] J. Simon, W. S. Bakr, R. Ma, M. E. Tai, P. M. Preiss, and M. Greiner, Nature (London) **472**, 307 (2011).
[10] X.-J. Liu, M. F. Borunda, X. Liu, and J. Sinova, Phys. Rev. Lett. **102**, 046402 (2009).
[11] Y.-J. Lin, R. L. Compton, A. R. Perry, W. D. Phillips, J. V. Porto, and I. B. Spielman, Phys. Rev. Lett. **102**, 130401 (2009).
[12] C. Wang, C. Gao, C.-M. Jian, and H. Zhai, Phys. Rev. Lett. **105**, 160403 (2010).
[13] Y.-J. Lin, K. Jimenez-Garcia, and I. B. Spielman, Nature (London) **471**, 83 (2011).
[14] T.-L. Ho and S. Zhang, Phys. Rev. Lett. **107**, 150403 (2011).
[15] W. Cong-Jun, I. Mondragon-Shem, and Z. Xiang-Fa, Chin. Phys. Lett. **28**, 097102 (2011).
[16] J. Dalibard, F. Gerbier, G. Juzeliūnas, and P. Öhberg, Rev. Mod. Phys. **83**, 1523 (2011).
[17] D. L. Campbell, G. Juzeliunas, and I. B. Spielman, Phys. Rev. A **84**, 025602 (2011).
[18] L. W. Cheuk, A. T. Sommer, Z. Hadzibabic, T. Yefsah, W. S. Bakr, and M. W. Zwierlein, Phys. Rev. Lett. **109**, 095302 (2012).
[19] P. Wang, Z.-Q. Yu, Z. Fu, J. Miao, L. Huang, S. Chai, H. Zhai, and J. Zhang, Phys. Rev. Lett. **109**, 095301 (2012).
[20] Y. Li, L. P. Pitaevskii, and S. Stringari, Phys. Rev. Lett. **108**, 225301 (2012).
[21] V. Galitski and I. B. Spielman, Nature (London) **494**, 49 (2013).
[22] C. Qu, C. Hamner, M. Gong, C. Zhang, and P. Engels, Phys. Rev. A **88**, 021604 (2013).
[23] C. Hamner, C. Qu, Y. Zhang, J. Chang, M. Gong, C. Zhang, and P. Engels, Nat. Commun. **5**, 4023 (2014).
[24] K. Jiménez-García, L. J. LeBlanc, R. A. Williams, M. C. Beeler, C. Qu, M. Gong, C. Zhang, and I. B. Spielman, Phys. Rev. Lett. **114**, 125301 (2015).
[25] J. Li, W. Huang, B. Shteynas, S. Burchesky, F. C. Top, E. Su, J. Lee, A. O. Jamison, and W. Ketterle, Phys. Rev. Lett. **117**, 185301 (2016).
[26] Z. Wu, L. Zhang, W. Sun, X.-T. Xu, B.-Z. Wang, S.-C. Ji, Y. Deng, S. Chen, X.-J. Liu, and J.-W. Pan, Science **354**, 83 (2016).
[27] L. Huang, Z. Meng, P. Wang, P. Peng, S.-L. Zhang, L. Chen, D. Li, Q. Zhou, and J. Zhang, Nat. Phys. **12**, 540 (2016).
[28] I. Dzyaloshinsky, J. Phys. Chem. Solids **4**, 241 (1958).
[29] T. Moriya, Phys. Rev. **120**, 91 (1960).
[30] I. A. Sergienko and E. Dagotto, Phys. Rev. B **73**, 094434 (2006).
[31] K. Cao, G.-C. Guo, D. Vanderbilt, and L. He, Phys. Rev. Lett. **103**, 257201 (2009).
[32] S. Mühlbauer, B. Binz, F. Jonietz, C. Pfleiderer, A. Rosch, A. Neubauer, R. Georgii, and P. Böni, Science **323**, 915 (2009).
[33] M. Mochizuki, N. Furukawa, and N. Nagaosa, Phys. Rev. Lett. **104**, 177206 (2010).
[34] Y. Tokura and S. Seki, Adv. Mater. **22**, 1554 (2010).
[35] X. Z. Yu, Y. Onose, N. Kanazawa, J. H. Park, J. H. Han, Y. Matsui, N. Nagaosa, and Y. Tokura, Nature (London) **465**, 901 (2010).
[36] S. Heinze, K. von Bergmann, M. Menzel, J. Brede, A. Kubetzka, R. Wiesendanger, G. Bihlmayer, and S. Blugel, Nat. Phys. **7**, 713 (2011).
[37] S. Seki, X. Z. Yu, S. Ishiwata, and Y. Tokura, Science **336**, 198 (2012).
[38] N. Nagaosa and Y. Tokura, Nat. Nano **8**, 899 (2013).
[39] M. N. Wilson, A. B. Butenko, A. N. Bogdanov, and T. L. Monchesky, Phys. Rev. B **89**, 094411 (2014).
[40] J. Radić, A. Di Ciolo, K. Sun, and V. Galitski, Phys. Rev. Lett. **109**, 085303 (2012).
[41] W. S. Cole, S. Zhang, A. Paramekanti, and N. Trivedi, Phys. Rev. Lett. **109**, 085302 (2012).
[42] M. Gong, Y. Qian, M. Yan, V. W. Scarola, and C. Zhang, Sci. Rep. **5**, 10050 (2015).
[43] U. Roszler, A. N. Bogdanov, and C. Pfleiderer, Nature (London) **442**, 797 (2006).
[44] J. Rowland, S. Banerjee, and M. Randeria, Phys. Rev. B **93**, 020404 (2016).
[45] L. He, A. Ji, and W. Hofstetter, Phys. Rev. A **92**, 023630 (2015).
[46] F. Sun, J. Ye, and W.-M. Liu, Phys. Rev. A **92**, 043609 (2015).
[47] F. Sun, J. Ye, and W.-M. Liu, New J. Phys. **19**, 063025 (2017).
[48] N. Schuch, M. M. Wolf, F. Verstraete, and J. I. Cirac, Phys. Rev. Lett. **100**, 040501 (2008).
[49] G. Vidal, Phys. Rev. Lett. **91**, 147902 (2003).
[50] F. Verstraete and J. I. Cirac, arXiv:cond-mat/0407066.
[51] A. W. Sandvik and G. Vidal, Phys. Rev. Lett. **99**, 220602 (2007).
[52] J.-P. Song and R. T. Clay, Phys. Rev. B **89**, 075101 (2014).
[53] Z. Wang, Y. Han, G.-C. Guo, and L. He, Phys. Rev. B **88**, 121105 (2013).
[54] S. Zhang, W. S. Cole, A. Paramekanti, and N. Trivedi, Ann. Rev. Cold Atoms Mol. **3**, 135 (2015).
[55] S.-J. Dong, W. Liu, X.-F. Zhou, G.-C. Guo, Z.-W. Zhou, Y.-J. Han, and L. He, Phys. Rev. B **96**, 045119 (2017).
[56] W. Liu, C. Wang, Y. Li, Y. Lao, Y. Han, G.-C. Guo, and L. He, J. Phys.: Condens. Matter **27**, 085601 (2015).

[57] R. H. Swendsen and J.-S. Wang, Phys. Rev. Lett. **57**, 2607 (1986).
[58] C. J. Geyer, Computer Science and Statistics, in *Proceedings of the 23rd Symposium on the Interface* (Interface Foundation, Seattle, Washington, 1991).
[59] J. Villain, R. Bidaux, J.-P. Carton, and R. Conte, J. Phys. **41**, 1263 (1980).
[60] E. F. Shender, Sov. Phys. JETP **56**, 178 (1982).
[61] Z. Nussinov and J. van den Brink, Rev. Mod. Phys. **87**, 1 (2015).
[62] J. Dorier, F. Becca, and F. Mila, Phys. Rev. B **72**, 024448 (2005).
[63] W.-L. You, G.-S. Tian, and H.-Q. Lin, J. Phys. A **43**, 275001 (2010).
[64] W. Brzezicki and A. M. Oleś, Phys. Rev. B **87**, 214421 (2013).
[65] I. Kézsmárki, S. Bordács, P. Milde, E. Neuber, L. Eng, J. White, H. M. Rønnow, C. Dewhurst, M. Mochizuki, K. Yanai *et al.*, Nat. Mater. **14**, 1116 (2015).
[66] T. Holstein and H. Primakoff, Phys. Rev. **58**, 1098 (1940).